scientific reports

Check for updates

OPEN

Network pharmacology and experimental validation reveal dexmedetomidine's protective mechanisms against acute liver injury in mice

Chong Zhang[1], Yixin Fan[2], Zhijun Qin[1], Mi Su[1] & Fu Yao[1]✉

This study explored the role and molecular mechanisms of dexmedetomidine (DEX), an α2-adrenergic receptor agonist, in the treatment of a mouse model of acute liver injury (ALI). DEX significantly mitigated hepatic tissue damage and reduced serum levels of liver function biomarkers and proinflammatory cytokines. Network pharmacology analysis revealed 81 common targets between DEX and ALI, identifying 10 crucial hub genes. Kyoto Encyclopedia of Genes and Genomes pathway analysis indicated that DEX's therapeutic effect on ALI is likely linked to the activation of the PI3K/AKT pathway. Immunohistochemical experiments verified DEX's activation of the PI3K/AKT pathway. Molecular docking and dynamic simulations confirmed the stable interaction between DEX and the epidermal growth factor receptor (EGFR). Immunohistochemistry and western blotting further validated that DEX pretreatment upregulated EGFR expression. Our findings indicate that DEX may mitigate ALI by interacting with EGFR and triggering the PI3K/AKT pathway. These findings provide a solid theoretical and experimental basis for using DEX as a potential therapeutic regimen for treating inflammatory liver diseases.

Keywords Dexmedetomidine, Network pharmacology, Acute liver injury, Phosphatidylinositol 3-kinase/protein kinase B, Epidermal growth factor receptor

Abbreviations

ALI	Acute liver injury
DEX	Dexmedetomidine
LPS	Lipopolysaccharide
IL	Interleukin
NF-κB	Nuclear factor-κB
PASMC	Pulmonary artery smooth muscle cell
D-Gal	D-galactose
SIL	Silibinin
ALT	Alanine transaminase
AST	Aspartate transaminase
TNF-α	Tumor necrosis factor-alpha
PI3K	Phosphatidylinositol 3-kinase
AKT	Protein kinase B
EGFR	Epidermal growth factor receptor
p-PI3K	Phosphorylated PI3K
p-AKT	Phosphorylated AKT
GAPDH	Glyceraldehyde-3-phosphate dehydrogenase
DHE	Dihydroethidium
PBS	Phosphate-buffered saline

[1]Department of Anesthesia, Sichuan Provincial Orthopedic Hospital (Chengdu Sports Hospital and Chengdu Research Institute for Sports Injury), Chengdu, China. [2]Oncology Department, Chengdu BOE Hospital, Chengdu, China. ✉email: yaofuyzk@163.com

OD	Optical density
H&E	Hematoxylin and eosin
TBST	Tris-buffered saline with Tween-20
PPI	Protein–protein interaction
CC	Cellular component
MF	Molecular function
BP	Biological process
KEGG	Kyoto Encyclopedia of Genes and Genomes
GO	Gene ontology
ROS	Reactive oxygen species
ALF	Acute liver failure

Acute liver injury (ALI) is a severe clinical condition caused by multiple factors that poses a significant threat to affected individuals. Its pathogenesis comprises diverse etiologies, including sepsis-induced hepatotoxic accumulation, improper drug use, chronic alcohol abuse, complications of metabolic syndrome, and hepatitis infections[1–5]. These factors, either individually or synergistically, damage hepatocytes, triggering complex physiological and pathological cascades. Despite substantial research efforts exploring ALI treatment strategies, including pharmacotherapy, nutritional support, and artificial liver support systems, a highly efficacious and safe therapeutic agent remains elusive[6]. Consequently, drugs that can effectively safeguard the liver, mitigate injury, and exhibit minimal side effects are urgently needed. These would not only offer safer and more effective treatment options for patients with ALI, but also provide new avenues for liver disease management.

Dexmedetomidine (DEX) is a widely used α2-adrenergic receptor agonist, known for its pronounced analgesic effects in surgical procedures and intensive care[7]. DEX has anti-inflammatory properties that can prevent organ damage associated with inflammation. In a rat model of myocardial ischemia/reperfusion injury, DEX mitigated myocardial damage by activating the Notch signaling pathway[8]. In a cellular model established using oxygen–glucose deprivation/reperfusion, DEX inhibited inflammatory damage[8]. In human microglial HMC3 cells, DEX significantly inhibited the production of interleukin (IL)-6 and IL-8 in both lipopolysaccharide (LPS)-stimulated and unstimulated conditions, indicating notable anti-inflammatory effects[9]. In human pulmonary artery smooth muscle cells (PASMCs) treated with fibroblast growth factor 2, DEX reduced IL-6 mRNA expression and inhibited proliferation by blocking NF-κB activation, thereby improving pulmonary hypertension[10]. Notably, DEX exhibited significant anti-inflammatory effects in critically ill patients[11,12]. We hypothesized that DEX could also safeguard the liver against inflammatory damage based on these findings.

In recent years, rapid advancements in bioinformatics and computational sciences have led to the emergence of network pharmacology as a novel pharmacology subdomain, showing unparalleled academic merit in drug discovery[13,14]. The construction of complex networks of drug–disease–biomolecule interactions facilitates the systematic analysis of drug efficacy mechanisms. Nowadays, network pharmacology has become a critical tool in elucidating these mechanisms[15,16]. This study utilized network pharmacology techniques to identify potential targets of DEX in ALI. We investigated the molecular mechanisms of DEX's therapeutic effects on liver injury and validated these findings through in vivo experiments. Our findings not only deepen our understanding of the pharmacological actions of DEX, but also provide a solid scientific foundation and theoretical basis for the application of DEX in liver disease therapies.

Materials and methods

Experimental reagents

LPS, DEX, D-galactose (D-Gal), and silibinin (SIL) were acquired from Sigma-Aldrich (Shanghai, China). ALT and AST detection kits were obtained from Nanjing Jiancheng Bioengineering Institute. Mouse cytokine detection kits for TNF-α, IL-6, IL-8 (CXCL1), and IL-1β were procured from Solarbio Science & Technology Co., Ltd. For protein expression analysis, antibodies targeting PI3K, AKT, EGFR, their phosphorylated forms (p-PI3K, p-AKT, p-EGFR), and GAPDH, were obtained from Abcam. Dihydroethidium (DHE) was procured from Shanghai Biotech Co. Ltd. All reagents and antibodies were utilized following the manufacturers' guidelines.

Experimental animals

C57BL/6 mice (eight-week-old, male, 22–25 g) were obtained from Chengdu Dashuo Experimental Animal Co., Ltd. (Chengdu, China). Animals were housed at an ambient temperature of 22 ± 2 °C under a fixed 12 h light/dark cycle. The animal experimentation protocol received ethical clearance and approval from the Experimental Animal Ethics Committee of Chengdu Medical College. All animal studies adhered to the ARRIVE 2.0 requirements, which included study design, animal numbers, randomization, and statistical methods. Prior to experimentation, animals were randomly assigned into seven groups (n = six per group): Control (Con), ALI model, DEX (administered 200 μg/kg DEX), and four ALI intervention groups treated with varying doses of DEX [ALI + DEX(L): 50 mg/kg, ALI + DEX(M): 100 mg/kg, ALI + DEX(H): 200 mg/kg] or SIL [ALI + SIL: 100 mg/kg]. The ALI model was induced by intraperitoneally injecting LPS/D-Gal (200 μL; 30 μg/kg; 600 mg/kg) dissolved in PBS. DEX and SIL were administered intraperitoneally 1 h prior to the LPS/D-Gal challenge. At 6 h after LPS/D-Gal treatment, the mice were then anesthetized with isoflurane and subjected to enucleation for exsanguination. Subsequently, the liver tissues were harvested, fixed with formalin, and embedded in paraffin.

Quantitative assessment of ALT and AST activities

ALT and AST activities in serum were measured using a standardized assay protocol as per the manufacturer's guidelines. After the chemical reaction reached its predefined endpoint, the optical density (OD) of each sample

was measured at 505 nm. Subsequently, the OD values were converted to the respective ALT and AST activities in each sample.

Quantitative analysis of inflammation cytokines in mouse serum

Specialized detection kits were used to quantitatively assess TNF-α, IL-6, IL-8, and IL-1β levels in mouse serum samples, following the manufacturer's instructions to ensure assay accuracy and reproducibility. After the reaction reached its predefined endpoint, the OD of each sample was measured at 450 nm, quantifying the inflammatory response in each mouse serum sample.

Pathological examination of mouse liver tissues

The left lateral lobe of the mouse liver was selectively isolated for subsequent experiments. To facilitate histological analysis, the liver tissues underwent a series of rigorous preservation steps, including formalin fixation, dehydration through graded ethanol solutions, and final embedding in paraffin wax. Subsequently, 4-μm-thick liver tissue sections were stained with hematoxylin and eosin (H&E) to enhance cellular and tissue morphology visualization. A comprehensive evaluation of the extent of liver damage was conducted under an optical microscope, allowing for a precise evaluation of any pathological alterations.

DHE staining to assess reactive oxygen species (ROS) levels in liver tissue

To visualize ROS production within the liver tissue, tissue sections were incubated with 5 μM of DHE working solution at 37 °C (30 min). The DHE-incubated sections were then examined and imaged under a fluorescence microscope, enabling the qualitative analysis of ROS generation within the liver tissue.

Immunohistochemistry

After deparaffinization and rehydration, liver tissue sections underwent antigen retrieval to enhance antibody accessibility. Liver tissue sections were incubated at 4 °C with antibodies against PI3K, AKT, EGFR, p-PI3K, and p-AKT, each diluted at 1:50 for optimal binding for 24 h. Sections were rinsed with phosphate-buffered saline (PBS) (3 × 3), then incubated with secondary antibodies for 50 min at 25 °C. Following additional PBS rinses, sections were stained with DAB. Sections were counterstained to enhance contrast and then mounted onto slides for microscopic observation. The expression levels and localization patterns of PI3K, AKT, EGFR, p-PI3K, and p-AKT in liver tissue were meticulously examined and documented using a microscope.

Western blot analysis of total liver tissue protein

Total protein samples from mouse liver tissue were separated using polyacrylamide gel (10%) electrophoresis and membrane transfer was carried out at a constant current of 250 mA for 2 h. The membranes were incubated with 5% skimmed milk (25 °C, 30 min), and then incubated with antibodies against EGFR (1:1000) and GAPDH (1:5000) as a loading control (4 °C, 24 h). Following TBST washing, secondary antibodies (1:5000) were incubated for 1 h at 27 °C. Following additional TBST washes, protein expression was visualized using enhanced chemiluminescence and captured using an imaging system. Band intensities were analyzed using the ImageJ software (v1.53q; https://imagej.net/software/imagej/), and protein expression was normalized to GAPDH levels.

Prediction of potential DEX targets

The standardized canonical SMILES string and 3D chemical structure (SDF format) of DEX were retrieved from the PubChem database using the keyword 'dexmedetomidine'. To comprehensively identify potential targets of DEX, we utilized five distinct online prediction platforms: PharmMapper, SwissTarget, ChemMapper (via TargetNet), the legacy version of SEA, and SuperTarget.

Target prediction for ALI

Genes linked to ALI were identified through OMIM (https://www.omim.org/, 'Approved Symbol') and GeneCards (https://www.genecards.org/, 'score' > 15) using the keyword 'acute liver injury'. The retrieved genes were mapped to gene names using the UniProt database.

Enrichment analyses of common genes were conducted using Gene Ontology and KEGG pathways.

We performed an enrichment analysis using the ClusterProfiler package (v4.4.4, https://bioconductor.org/packages/3.17/bioc/html/clusterProfiler.html) for Homo sapiens in the R statistical software environment (v4.2.1, https://cran.r-project.org/bin/windows/base/old/4.2.1/) to understand the functional roles and biological pathways of the common genes identified between ALI-related genes and DEX targets. This analysis utilized the GO and KEGG databases to investigate the overrepresentation of particular biological processes (BPs), molecular functions (MFs), cellular components (CCs), and metabolic/signaling pathways among these common genes[17–19]. The org.Hs.eg.db package was employed to facilitate the conversion of gene identifiers into a consistent format, ensuring compatibility with the enrichment analysis tools. Subsequently, a Venn diagram analysis was performed to visually identify and enumerate the genes shared between the ALI-associated gene set and predicted DEX targets.

Hub targeting analysis

We utilized the STRING database (https://www.string-db.org/) to construct a comprehensive protein–protein interaction (PPI) network, aiming to elucidate the interconnectivity and potential functional roles of the identified shared targets. The shared targets were uploaded to STRING, and the resulting PPI data was imported

into Cytoscape (v3.9.1, https://cytoscape.org/) for visualization and analysis. The degree centrality metric in Cytoscape was utilized to evaluate the significance of individual proteins. To identify hub genes, the CytoHubba plugin, a powerful tool for ranking nodes in Cytoscape networks based on various topological features, was used, specifically focusing on degree centrality. The identified hub genes provided insights into the core regulatory components, potentially playing roles in the relevant biological processes.

Molecular docking analysis

Prior to docking, these structures underwent preprocessing in AutoDockTools (v1.5.6, http://autodock.scripps.edu/), which involved the elimination of crystallographic water molecules and incorporation of hydrogen atoms to ensure accurate simulation conditions. Molecular docking simulations were performed using AutoDock Vina (v1.1.2,http://vina.scripps.edu/). The resulting docking poses were subsequently visualized and analyzed using Pymol (v2.1, https://pymol.org/) and Discovery Studio (DS) (DS2019, https://www.3ds.com/products-services/biovia/), providing insights into the spatial arrangements and interactions within the ligand-receptor complexes. The strength of these interactions was evaluated by calculating the binding free energy.

Molecular dynamics simulations

To gain insights into the dynamic behavior of the selected receptor-ligand complexes, molecular dynamics simulations were carried out (Gromacs 2020 software package, https://www.gromacs.org). The AMBER99SB-ILDN force field was used for protein components. Small molecule ligands were modeled using the General Amber Force Field (GAFF). The topology of ligands was constructed using the Sobtop program. Furthermore, atomic charges were optimized using the RESP method to refine electrostatic interactions within the system. The TIP3P explicit water model was used, ensuring a minimum distance of 1.0 nm between protein atoms and the water box boundaries. Based on the preliminary docking results, appropriate amounts of sodium or chloride ions were introduced into the system to neutralize its overall charge, ensuring electrostatic neutrality during simulations. The simulation protocol comprised four distinct stages: energy minimization to relieve local stresses, heating to gradually increase the system temperature, equilibration to reach a steady state, and finally, production dynamics to capture the dynamic properties of the receptor-ligand complexes. Initially, the heavy atoms of the protein and ligand were constrained, while the water molecules underwent 10,000 steps of energy minimization, consisting of 5,000 steepest descents and 5,000 conjugate gradients. Subsequently, the entire system was subjected to an additional 10 000 steps of energy minimization. Equilibration was performed for 50 ps under the NPT ensemble conditions. Binding free energies were calculated using the gmx_MMPBSA method implemented in Gromacs 2020.

Statistical analysis

All data were rigorously analyzed using GraphPad Prism 7.0 software (https://www.graphpad.com). To assess the statistical significance of the observed differences, both t-tests and analyses of variance (ANOVA) were employed. Statistical significance was set at $p < 0.05$. To further strengthen the reliability and reproducibility of the findings, each experiment was independently replicated at least three times.

Results

DEX attenuated oxidative stress and inflammatory response

To validate the hepatoprotective effects of DEX against ALI, we performed histopathological evaluation of liver tissues. As expected, the ALI model group exhibited pronounced pathological alterations in hepatocytes, featuring extensive necrosis, nuclear fragmentation, dissolution, and cytoplasmic disintegration, accompanied by inflammatory cell infiltration (Fig. 1A). Notably, treatment with silymarin and high-dose DEX (DEX-H) markedly ameliorated these pathological changes (Fig. 1A). In the ALI model group, elevated serum ALT and AST levels indicated impaired liver function. Mice in the DEX group showed lower levels of ALT and AST, indicating DEX's hepatoprotective effect (Fig. 1B,C). We performed ELISA to quantify the serum levels of key inflammatory cytokines to assess the effect of DEX on the inflammatory response. The ALI model group showed significant elevations in serum IL-6, IL-8, IL-1β, and TNF-α levels. Conversely, DEX administration markedly attenuated these effects (Fig. 1D–G). Moreover, DHE staining revealed a surge in ROS-positive cells in the ALI model group, indicating oxidative stress. However, DEX treatment markedly reduced the number of ROS-positive cells (Fig. 1H,I).

Molecular mechanism of ALI alleviation by DEX as revealed using network pharmacology

Database analysis identified 400 DEX targets and 997 disease targets, with 81 potential targets for DEX-mediated ALI treatment (Fig. 2A). We conducted enrichment analysis of potential DEX–ALI targets, concentrating on CCs, MFs, and BPs. Figure 2B highlights the top 10 BPs, such as response to xenobiotic stimulus, positive regulation of kinase activity, Pi3k/AKT signaling, phosphatidylinositol-mediated signaling, and other BPs associated with kinase regulation, lipid metabolism, and extracellular stimulus response. The top 10 CCs included membrane rafts, microdomains, vesicle lumens, focal adhesions, cell–substrate junctions, and neuronal structures, the subcellular localization of which is shown in Fig. 2C. Likewise, the top 10 MFs comprised kinase activities (serine/threonine/tyrosine), heme/tetrapyrrole binding, RNA polymerase II transcription factor binding, transmembrane receptor activities, and exogenous protein binding, the functional roles of which are illustrated in Fig. 2D. Figure 2E highlights the top 10 enriched KEGG pathways, including PI3K-AKT signaling, lipid and atherosclerosis, Ras and MAPK signaling, Rap1 signaling, cancer-related pathways, and pathways linked to ROS, atherosclerosis, and viral infections. Finally, we generated a Sankey bubble plot of the top five enriched KEGG pathways, which visually illustrates the intricate gene–pathway relationships (Fig. 2F), offering insights into the mechanisms behind DEX's therapeutic effects in ALI.

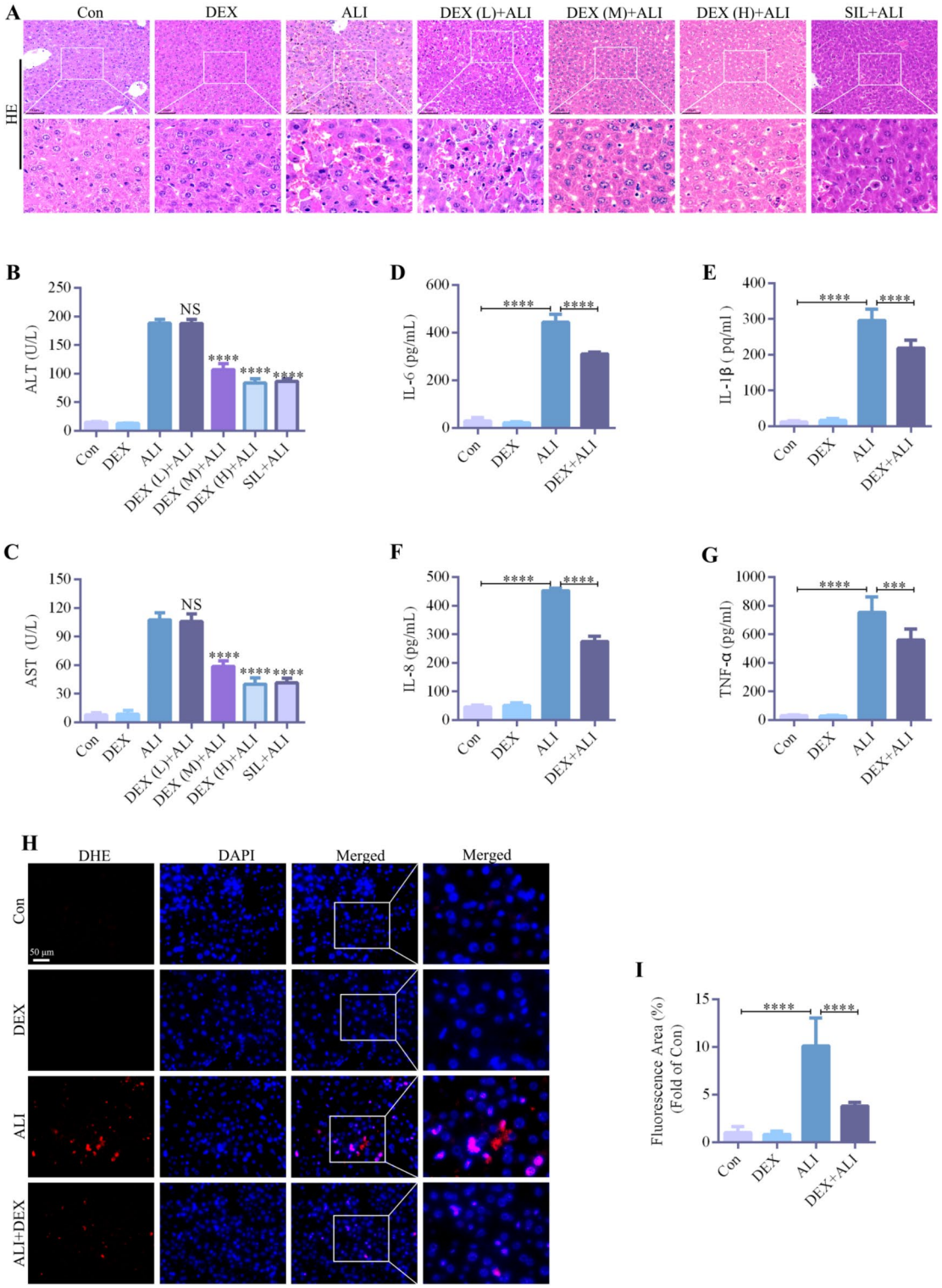

Fig. 1. Dexmedetomidine alleviates oxidative stress and inflammation in mouse liver. (**A**) H&E staining illustrating histopathological alterations; scale bar = 50 μm. (**B**,**C**) Quantification of ALT and AST in mouse serum. (**D**–**G**) Quantification of IL-6, IL-1β, IL-8, and TNF-α in mouse serum. (**H**) DHE fluorescence staining revealing oxidative stress in liver tissues. (**I**) Quantitative DHE analysis. Data are shown as mean ± SD (n = 6). $^{*}p < 0.05$, $^{**}p < 0.01$, $^{***}p < 0.001$, $^{****}p < 0.0001$ compared to the ALI group. Groups: Con (control), ALI (acute liver injury), DEX (dexmedetomidine), SIL (silymarin). NS denotes nonsignificant differences.

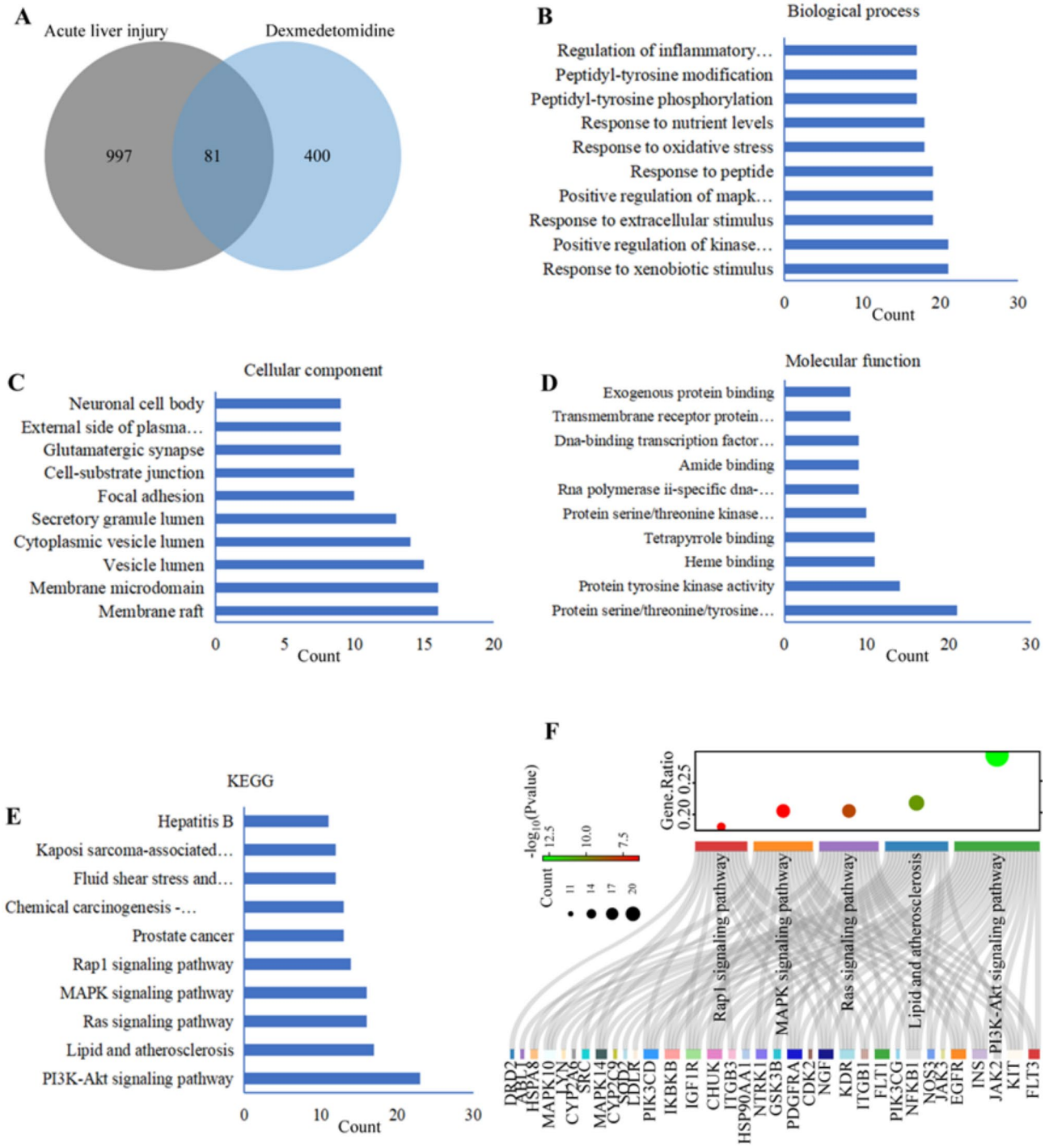

Fig. 2. Network pharmacology revealing molecular mechanisms of ALI alleviation by DEX. (**A**) A Venn diagram depicting the common targets between dexmedetomidine (DEX) and ALI, highlighting potential therapeutic candidates for DEX in ALI treatment. (**B**–**D**) Results of GO enrichment analysis for BPs, CCs, and MFs. (**E**) KEGG pathway analysis was conducted on the 81 potential therapeutic targets to explore the biological pathways involved. (**F**) Sankey bubble plot visualizing the top five enriched KEGG pathways.

DEX activated the PI3K-AKT pathway to alleviate ALI in mice

The KEGG pathway analysis identified the 'PI3K-AKT signaling pathway' as the most enriched pathway, highlighting its critical role in ALI progression. We employed immunohistochemical staining and western blotting to evaluate PI3K, AKT, p-PI3K, and p-AKT expression, aiming to determine if DEX mitigates ALI by activating this pathway. In the ALI model, the expression levels of PI3K, AKT, p-PI3K, and p-AKT were significantly downregulated compared to the Con group (Fig. 3A–K). DEX treatment significantly upregulated

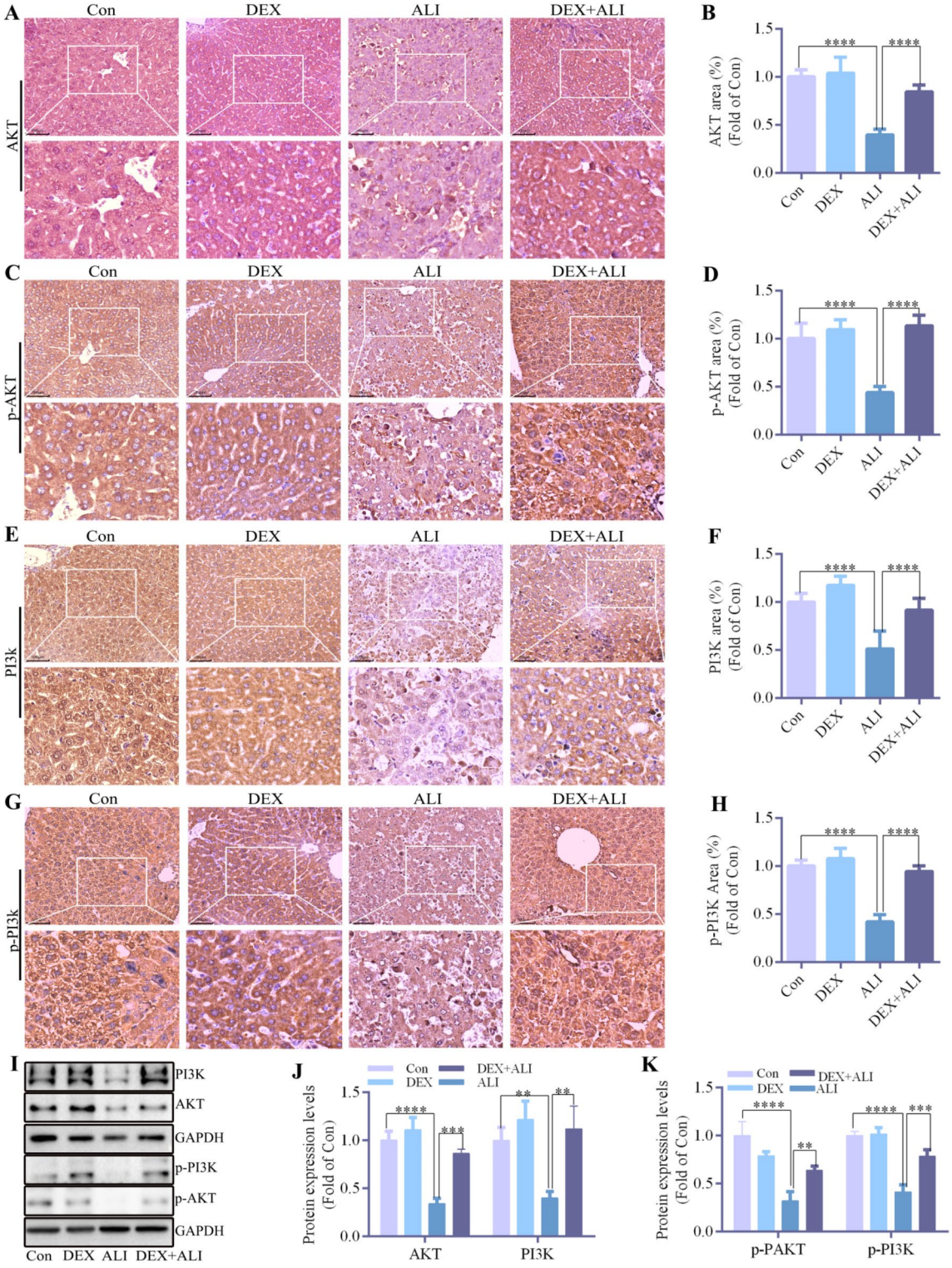

Fig. 3. DEX alleviates ALI in mice by activating the PI3K-AKT pathway. (**A**) Immunohistochemical analysis of AKT levels in mouse liver tissues. (**B**) Quantitative assessment of AKT staining. (**C**) Immunohistochemical analysis of the levels of p-AKT (phosphorylated AKT) in mouse liver tissues. (**D**) Quantitative evaluation of p-AKT staining. (**E**) Immunohistochemical analysis of the levels of PI3K (phosphatidylinositol 3-kinase) in mouse liver tissues. (**F**) Quantitative analysis of PI3K staining. (**G**) Immunohistochemical analysis of p-PI3K levels in mouse liver tissues. (**H**) Quantitative assessment of p-PI3K staining. (**I**) Western blotting analysis of AKT, PI3K, p-AKT and p-PI3K levels in mouse liver tissues. (**J**,**K**) Quantitative analysis of AKT, PI3K, p-AKT and p-PI3K. Scale bar = 100 μm; Data are expressed as mean ± standard deviation (n = 6). $^{*}p < 0.05$, $^{**}p < 0.01$, $^{***}p < 0.001$, $^{****}p < 0.0001$. Con: control group; ALI: acute liver injury group; DEX: dexmedetomidine group; SIL: silymarin group.

the expression of these proteins, suggesting that DEX may ameliorate ALI through PI3K-AKT pathway activation (Fig. 3A–K).

Pinpointing potential DEX therapeutic targets in ALI through PPI assessment and molecular docking strategies

To elucidate the mechanisms by which DEX alleviates ALI, we constructed a PPI network encompassing 81 potential targets with 80 nodes and 699 edges (Fig. 4A). By employing the Maximum Clique Centrality (MCC) algorithm in CytoHubba, we identified the top 10 crucial targets of DEX in ALI therapy: EGFR, INS, NFKB1, SRC, ALB, HSP90AA1, IGF1R, PARP, PTGS2, and KIT (Fig. 4B). To explore the connection between these targets and the PI3K-AKT pathway, we constructed a Venn diagram and compared targets enriched in the PI3K-AKT pathway with the top 10 MCC-ranked targets. We accordingly identified six vital therapeutic targets in ALI: EGFR, KIT, NFKB1 (NFKB), IGF1R (IGFE1R), HSP90AA1 (Hsp90aa1), and INS (Fig. 4C). To validate our bioinformatics predictions, we conducted molecular docking simulations between DEX and these six targets. The docking results revealed binding free energies of − 5.9 kcal/mol (EGFR), − 5.13 kcal/mol (KIT), − 4.98 kcal/mol (NFKB), − 4.95 kcal/mol (IGFE1R), − 4.84 kcal/mol (Hsp90aa1), and − 4.72 kcal/mol (INS) (Fig. 4D–I). In particular, lower binding free energies indicate a stronger binding affinity. Remarkably, EGFR demonstrated the strongest binding affinity with DEX, suggesting a strong interaction that may underlie the crucial therapeutic effect of DEX against ALI.

Molecular dynamics simulations and in vivo experiments for validating the pharmacological targets of DEX in ALI

To delve deeper into small molecule–protein interactions, we conducted 100 ns molecular dynamics simulations. As indicated in the plots, the average RMSD of complexes remained below 6.2 A, achieving dynamic equilibrium at approximately 45 ns (Fig. 5A). RMSF analysis revealed minor conformational changes in a subset of amino acids (e.g., residues 720–740 and at approximately 830), whereas the majority exhibited tolerable fluctuations (Fig. 5B). The radius of gyration (Rg) plot showed stable Rg for the EGFR protein until 45 ns, followed by a pronounced decrease (Fig. 5C). The solvent-accessible surface area (SASA) plot indicated the occurrence of minimal changes during the first 20 ns, followed by a marked decline thereafter (Fig. 5D). The hydrogen bond networks between each protein and DEX exhibited strong interactions with the pocket amino acids (Fig. 5E).

We observed slight adjustments in the binding mode of the small molecule to the active site, maintaining hydrogen bonding with MET-795 and hydrophobic interactions with the surrounding residues (ALA-745, VAL-728, LEU-794, PRO-796, and LEU-720) (Fig. 5F–H). These interactions suggested a stable complex formation despite minor adjustments.

EGFR and p-EGFR expression in the ALI model group was significantly lower than that in normal mice. Conversely, DEX treatment significantly elevated EGFR and p-EGFR expression (Fig. 5I–K), indicating a strong DEX-EGFR interaction. We hypothesized that this interaction enhances EGFR/PI3K/AKT pathway activation, aiding in ALI improvement.

Discussion

Acute liver failure (ALF) involves significant hepatocyte death, marked by cellular content release, cell swelling, and inflammatory cytokine secretion[20]. The rapid deterioration of hepatic function can provoke a systemic inflammatory response, potentially leading to multiorgan failure and life-threatening conditions. Although liver transplantation remains the definitive clinical treatment for ALF, this is often hindered by scarce organ donations, organ rejection risks, and substantial treatment costs[21]. Therefore, the development of novel and efficacious therapeutic interventions is crucial for addressing this clinical challenge. Our study revealed the potential hepatoprotective mechanism of DEX, a drug that attenuates ROS generation, thereby inhibiting oxidative stress. DEX modulated inflammatory cytokine levels, thereby alleviating inflammation. Its protective effect against liver damage is mediated by activating the EGFR/PI3K/AKT pathway. This suggests that DEX may be used as a novel therapeutic strategy, with EGFR/PI3K/AKT pathway serving as a potential target for ALF treatment.

The LPS/d-GalN-induced ALI mouse model is a widely accepted and reliable mimic of clinical hepatitis for studying hepatoprotectant efficacy[22–27]. LPS triggers hepatocyte apoptosis and necrosis, whereas d-GalN, a hepatotoxic amino sugar, exacerbates liver damage. Their combined use increases hepatic sensitivity to LPS-mediated cytotoxicity, accelerating ALI progression. Consequently, this model was selected for in vivo evaluation of the anti-ALI properties of DEX. ALI model mice exhibited marked increases in the activity of serum ALT and AST, which are indicative of severe hepatic dysfunction. However, DEX effectively reversed these alterations, highlighting its potential hepatoprotective role. The accumulation and infiltration of inflammatory cells significantly contribute to hepatocyte death. H&E staining demonstrated that DEX significantly mitigated hepatic hemorrhage, necrosis, and inflammatory cell infiltration in ALI model mice, suggesting that DEX can efficiently alleviate LPS/D-GalN-induced pathological alterations in mouse liver tissue.

Accumulating evidence have highlighted oxidative stress and inflammation as pivotal pathogenic factors in ALF[28,29]. Diminished antioxidant defenses can intensify hepatic inflammation, leading to increased hepatocyte necrosis due to proinflammatory cytokines[30–32]. Thus, inhibiting ROS and inflammation may be a preventive strategy against ALI[33,34]. Our findings are consistent with those of others, which revealed that DEX significantly mitigated oxidative stress by restoring the balance between biochemical toxicity and ROS generation, indicating its antioxidant potential. DEX significantly mitigated inflammatory responses by downregulating inflammatory cytokines, demonstrating potent anti-inflammatory properties[35–37].

Through network pharmacology, a potent tool for predicting pharmacological actions[38,39], we revealed the underlying mechanisms of DEX in ALI. This methodology enabled us to devise a predictive model for deciphering

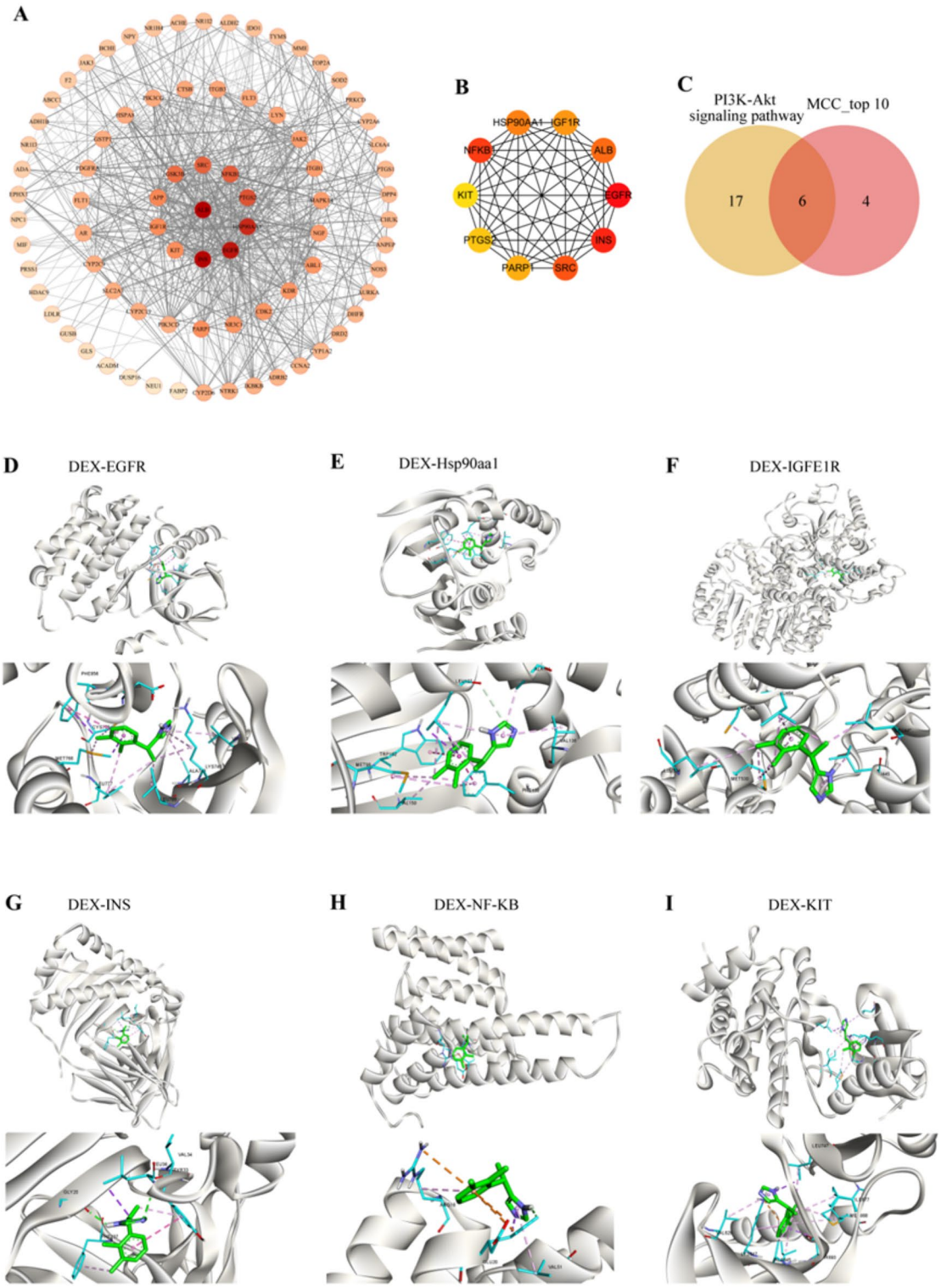

Fig. 4. Identification of potential DEX targets in ALI treatment. (**A**) Visualization of a PPI network comprising 81 cross-targets between DEX and ALI. The stronger the red hue suggesting greater centrality or significance within the network. (**B**) Ten crucial hub genes occupying pivotal positions in the interaction landscape in the PPI network. (**C**) Venn diagram illustrating the overlap between the PI3K-AKT pathway and the 10 hub genes in the PPI network, emphasizing their interconnections. (**D**–**I**) Three-dimensional images depicting the binding patterns of DEX with the following targets: EGF, KIT, NF-κB IGF1R, Hsp90aa1, and INS.

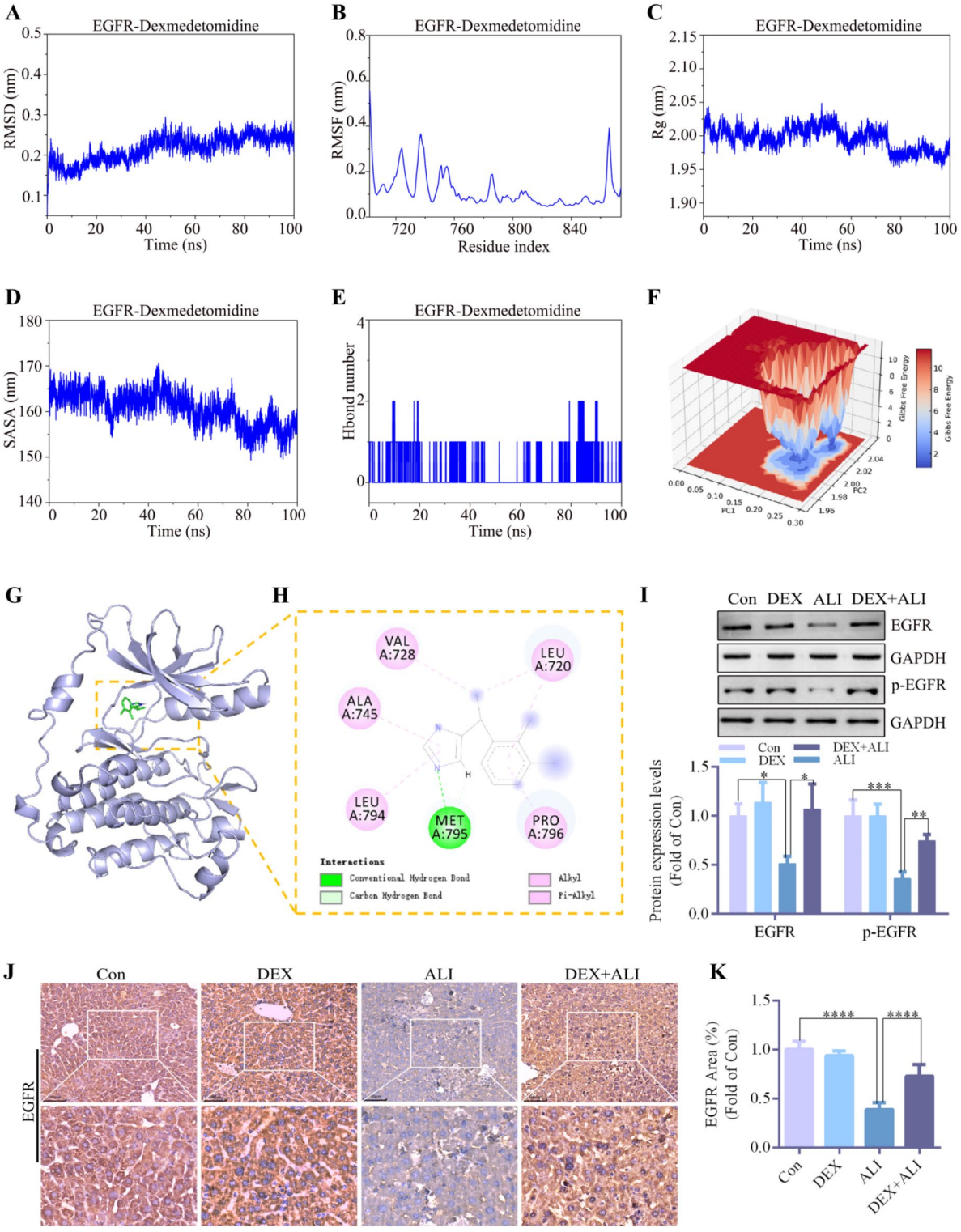

the specific mode of action of DEX in patients with ALI. GO and KEGG pathway analyses revealed DEX's crucial role in oxidative stress response to external stimuli and its hepatoprotective effects via the PI3K/AKT pathway. In vivo tests further affirmed the protective efficacy of DEX and its underlying molecular mechanism. Our data demonstrated increased expression of PI3K, AKT, and their phosphorylated forms, aligning with studies that suggest activation of the PI3K/AKT pathway inhibits apoptosis and organ damage. For instance, PI3K/AKT/AMPK upregulation mitigated liver injury in carbon tetrachloride-treated mice[40]. Fructus lycii oligosaccharides and leonurine alleviated liver damage via activation of the PI3K/AKT/mTOR pathway[41,42]. By combining molecular docking, dynamics simulations, and in vivo findings, we validated the strong affinity of DEX for EGFR, a crucial upstream activator of PI3K/AKT. EGFR activates the PI3K/AKT/mTOR pathway, which inhibits apoptosis[43]. These findings underscore DEX's potential therapeutic role in mitigating ALI through the EGFR/

◀**Fig. 5**. Molecular dynamics simulations and in vivo experiments for validating the pharmacological targets of DEX in ALI. (**A**) RMSD analysis of the EGFR-DEX complex from molecular dynamics simulations. (**B**) RMSF analysis of the EGFR-DEX complex from molecular dynamics simulations. (**C**) Radius of gyration (Rg) analysis of the EGFR-DEX complex in molecular dynamics simulations. (**D**) Solvent-accessible surface area (SASA) analysis of the EGFR-DEX complex in molecular dynamics simulations. (**E**) Hydrogen bond occupancy analysis during molecular dynamics simulations. (**F**) Three-dimensional structure of the EGFR-DEX complex. (**G**) Surface representation of the active site in the EGFR-DEX complex. (H) Detailed binding mode of the EGFR-DEX complex. (**I**) Western blot analysis of the levels of EGFR and p-EGFR; Quantitative analysis of EGFR and p-EGFR. (**J**) Immunohistochemical analysis of EGFR expression in mouse liver tissues. (**K**) Quantitative assessment of EGFR staining. Scale bar = 100 μm; Data are expressed as mean ± standard deviation (n = 6).*$p < 0.05$, **$p < 0.01$, ***$p < 0.001$, ****$p < 0.0001$. Con: control group; ALI: acute liver injury group; DEX: dexmedetomidine group; SIL: silymarin group.

PI3K/AKT pathway. However, this study has certain limitations. One of the main drawbacks was that we did not explore whether DEX acts through other targets.

In conclusion, our in vivo model highlighted the remarkable hepatoprotective benefits of DEX; while using network pharmacology we predicted that the EGFR/PI3K/AKT pathway is a mediator in the mechanism of action of DEX. In vivo validation confirmed that DEX mitigates ALI via the activation of the EGFR/PI3K/AKT pathway. These findings suggest that EGFR/PI3K/AKT agonists may represent potential therapeutic options for ALI, and that DEX holds promising application value in the clinical treatment of liver injury.

Data availability

The data supporting this study's findings are included in the article.

Received: 13 September 2024; Accepted: 11 March 2025
Published online: 17 March 2025

References

1. Dong, W. et al. Ceramide kinase-mediated C1P metabolism attenuates acute liver injury by inhibiting the interaction between KEAP1 and NRF2. *Exp. Mol. Med.* **56**, 946–958 (2024).
2. Niemietz, P. et al. C-C chemokine receptor type 7 (CCR7) regulates hepatic CD8 + T cell homeostasis and response to acute liver injury. *Hepatology (Baltimore, Md.)*, **80**, 1104–1119 (2024).
3. Wu, A. et al. Multienzyme active manganese oxide alleviates acute liver injury by mimicking redox regulatory system and inhibiting ferroptosis. *Adv. Healthc. Mater.* **13**, e2302556 (2024).
4. Zhang, Y. et al. Degradation of Angelica sinensis polysaccharide: Structures and protective activities against ethanol-induced acute liver injury. *Carbohydr. Polym.* **328**, 121745 (2024).
5. Zhao, T. et al. Pregnane X receptor activation in liver macrophages protects against endotoxin-induced liver injury. *Adv. Sci. (Weinh).* **11**, e2308771 (2024).
6. Stravitz, R. T. et al. Future directions in acute liver failure. *Hepatology.* **78**, 1266–1289 (2023).
7. Yuan, D. et al. Activation of the α(2B) adrenoceptor by the sedative sympatholytic dexmedetomidine. *Nat. Chem. Biol.* **16**, 507–512 (2020).
8. Guo, P. et al. Dexmedetomidine alleviates myocardial ischemia-reperfusion injury by down-regulating miR-34b-3p to activate the Jagged1/Notch signaling pathway. *Int. Immunopharmacol.* **116**, 109766 (2023).
9. Yamazaki, S., Yamaguchi, K., Someya, A., Nagaoka, I. & Hayashida, M. Anti-inflammatory action of dexmedetomidine on human microglial cells. *Int. J. Mol. Sci.* **23**, 10096 (2022).
10. Yamaguchi, Y. et al. The anti-inflammatory effects and clinical potential of dexmedetomidine in pulmonary arterial hypertension. *J. Pharmacol. Exp. Ther.* **385**, 88–94 (2023).
11. Ueki, M. et al. The effects of dexmedetomidine on inflammatory mediators after cardiopulmonary bypass. *Anaesthesia.* **69**, 693–700 (2014).
12. Lankadeva, Y. R., Shehabi, Y., Deane, A. M., Plummer, M. P. & Bellomo, R. Emerging benefits and drawbacks of α(2) -adrenoceptor agonists in the management of sepsis and critical illness. *Br. J. Pharmacol.* **178**, 1407–1425 (2021).
13. Nogales, C. et al. Network pharmacology: Curing causal mechanisms instead of treating symptoms. *Trends Pharmacol. Sci.* **43**, 136–150 (2022).
14. Noor, F., Asif, M., Ashfaq, U. A., Qasim, M., & Tahir Ul Qamar, M. Machine learning for synergistic network pharmacology: a comprehensive overview. *Brief Bioinform.* **24**, bbad120 (2023).
15. Gu, Y. et al. Exploring the efficacious constituents and underlying mechanisms of sini decoction for sepsis treatment through network pharmacology and multi-omics. *Phytomedicine.* **123**, 155212 (2024).
16. Li, C., Lin, X., Lin, Q., Lin, Y. & Lin, H. Jiangu granules ameliorate postmenopausal osteoporosis via rectifying bone homeostasis imbalance: A network pharmacology analysis based on multi-omics validation. *Phytomedicine.* **122**, 155137 (2024).
17. Kanehisa, M. Toward understanding the origin and evolution of cellular organisms. *Protein Sci.* **28**, 1947–1951 (2019).
18. Kanehisa, M., Furumichi, M., Sato, Y., Kawashima, M. & Ishiguro-Watanabe, M. KEGG for taxonomy-based analysis of pathways and genomes. *Nucleic Acids Res.* **51**, D587–D592 (2023).
19. Kanehisa, M. & Goto, S. KEGG: Kyoto encyclopedia of genes and genomes. *Nucleic Acids Res.* **28**, 27–30 (2000).
20. Stockmann, H. B., Hiemstra, C. A., Marquet, R. L., & IJzermans, J. N. Extracorporeal perfusion for the treatment of acute liver failure. *Ann. Surg.* **231**, 460–470 (2000).
21. Tujios, S., Stravitz, R. T. & Lee, W. M. Management of acute liver failure: Update 2022. *Semin. Liver Dis.* **42**, 362–378 (2022).
22. Feng, J. et al. RNF115/BCA2 deficiency alleviated acute liver injury in mice by promoting autophagy and inhibiting inflammatory response. *Cell Death Dis.* **14**, 855 (2023).
23. Guo, P. et al. Isolation of calenduloside E from Achyranthes bidentata blume and its effects on LPS/D-GalN-induced acute liver injury in mice by regulating the AMPK-SIRT3 signaling pathway. *Phytomedicine.* **125**, 155353 (2024).
24. Tang, S. et al. The novel hepatoprotective mechanisms of silibinin-phospholipid complex against d-GalN/LPS-induced acute liver injury. *Int. Immunopharmacol.* **116**, 109808 (2023).
25. Zeng, M., Feng, A., Wang, L., Li, K., & Zhou, J. Aralia saponin A isolated from Achyranthes bidentata Bl. ameliorates LPS/D-GalN induced acute liver injury via SPHK1/S1P/S1PR1 pathway in vivo and in vitro. *Int. Immunopharmacol.* **124**, 110912 (2023).

26. Zheng, X. et al. Eriodictyol alleviated LPS/D-GalN-induced acute liver injury by inhibiting oxidative stress and cell apoptosis via PI3K/AKT signaling pathway. *Nutrients* **15**, 4349 (2023).
27. Zhou, X. N. et al. Silent information regulator sirtuin 1 ameliorates acute liver failure via the p53/glutathione peroxidase 4/gasdermin D axis. *World J. Gastroenterol.* **30**, 1588–1608 (2024).
28. Guo, H. et al. Shikonin attenuates acetaminophen-induced acute liver injury via inhibition of oxidative stress and inflammation. *Biomed. Pharmacother.* **112**, 108704 (2019).
29. Luo, F. et al. Construction of phlorotannin-based nanoparticles for alleviating acute liver injury. *ACS Appl. Mater. Interfaces.* **15**, 47338–47349 (2023).
30. Rungratanawanich, W. et al. ALDH2 deficiency increases susceptibility to binge alcohol-induced gut leakiness, endotoxemia, and acute liver injury in mice through the gut-liver axis. *Redox. Biol.* **59**, 102577 (2023).
31. Wang, B. Cyanidin alleviated CCl(4)-induced acute liver injury by regulating the Nrf2 and NF-κB signaling pathways. *Antioxidants (Basel).* **11**, 2383 (2022).
32. Zhao, Q. et al. Celastrol ameliorates acute liver injury through modulation of PPARα. *Biochem. Pharmacol.* **178**, 114058 (2020).
33. Ding, X. & Fan, S. Purple sweet potato polysaccharide ameliorates concanavalin A-induced hepatic injury by inhibiting inflammation and oxidative stress. *Phytomedicine.* **129**, 155652 (2024).
34. Shearn, C. T. et al. Thioredoxin reductase 1 regulates hepatic inflammation and macrophage activation during acute cholestatic liver injury. *Hepatol. Commun.* **7**, e0020 (2023).
35. Yang, C. et al. Dexmedetomidine alleviated lipopolysaccharide/d-galactosamine-induced acute liver injury in mice. *Int. Immunopharmacol.* **72**, 367–373 (2019).
36. Tong, F. et al. Dexmedetomidine attenuates lipopolysaccharide-induced acute liver injury in rats by inhibiting caveolin-1 downstream signaling pathway. *Biosci. Rep.* **41**, BSR20204279 (2021).
37. Sha, J. et al. Dexmedetomidine improves acute stress-induced liver injury in rats by regulating mkp-1, inhibiting nf-κb pathway and cell apoptosis. *J. Cell. Physiol.* **234**, 14068–14078 (2019).
38. Gao, J., Yang, S., Xie, G., Pan, J. & Zhu, F. Integrating network pharmacology and experimental verification to explore the pharmacological mechanisms of aloin against gastric cancer. *Drug Des. Dev. Ther.* **16**, 1947–1961 (2022).
39. Zhang, H. et al. Bioinformatics and network pharmacology identify the therapeutic role and potential mechanism of melatonin in AD and Rosacea. *Front. Immunol.* **12**, 756550 (2021).
40. Zhang, S. et al. Metabolomics reveals that chronic restraint stress alleviates carbon tetrachloride-induced hepatic fibrosis through the INSR/PI3K/AKT/AMPK pathway. *J. Mol. Med. (Berl)* **102**, 113–128 (2024).
41. Wang, Z. et al. Fructus lycii oligosaccharide alleviates acute liver injury via PI3K/Akt/mTOR pathway. *Immunol. Res.* **72**, 271–283 (2024).
42. Yu, Y. et al. Leonurine alleviates acetaminophen-induced acute liver injury by regulating the PI3K/AKT signaling pathway in mice. *Int. Immunopharmacol.* **120**, 110375 (2023).
43. Geng, Z. et al. Ginkgetin improved experimental colitis by inhibiting intestinal epithelial cell apoptosis through EGFR/PI3K/AKT signaling. *FASEB J.* **38**, e23817 (2024).

Author contributions

"Conceptualization, Fu Yao and Chong Zhang.; methodology, Chong Zhang.; software, Yixin Fan.; validation,Zhijun Qin., and Mi Su.; formal analysis, Zhijun Qin.; investigation, Yixin Fan.; resources, Mi Su.; data curation, Mi Su.; writing—original draft preparation, Chong Zhang.; writing—review and editing, Fu Yao.; visualization, Chong Zhang.; supervision, Fu Yao.; project administration, Fu Yao.; funding acquisition, Fu Yao. All authors have read and agreed to the published version of the manuscript.

Funding

This research did not receive any specific funding.

Declarations

Competing interests

The authors declare no competing interests.

Ethics approval

All animal experiments were conducted in strict accordance with ethical guidelines, following formal authorization and approval from the Experimental Animal Ethics Committee of Chengdu Medical College.

Additional information

Supplementary Information The online version contains supplementary material available at https://doi.org/10.1038/s41598-025-93998-z.

Correspondence and requests for materials should be addressed to F.Y.